Review Article

Jan-Hendrik Klein-Wiele, Andreas Blumenstein, Peter Simon and Jürgen Ihlemann*

Laser interference ablation by ultrashort UV laser pulses via diffractive beam management

https://doi.org/10.1515/aot-2019-0068
Received December 2, 2019; accepted January 14, 2020; previously published online February 14, 2020

Abstract: The fabrication of periodic surface patterns on various materials by ultrashort ultraviolet (UV) laser pulses is reviewed. Laser interference ablation using two or more coherent beams leads to deterministic, strictly periodic patterns. The generation of the interfering beams is accomplished by diffractive optical elements like gratings, grating systems or computer-generated holograms. The recombination of the diffracted beams is performed by optical imaging or diffractive beam management. Ultrashort UV pulses are especially suited for generating micron- to submicron-sized deterministic periodic patterns on metals and semiconductors.

Keywords: diffractive beam management; laser interference ablation; submicron periodic patterns; ultrashort UV laser pulses.

1 Introduction

Periodic surface patterns on technical materials find numerous applications for marking [1], adjusting wettability [2], enhancing or lowering friction [3], enhancing solar cell efficiency [4] and many others. Especially patterns with periods ranging from a few hundred nanometers to a few microns are interesting, because they are optically effective in generating colorful surfaces. Conversely, optical methods are optimally suited to create such micron-sized patterns. Interference of two or multiple coherent light (laser) beams leads inevitably to periodic intensity patterns, which can be utilized to create corresponding structural patterns on a material surface. This can be accomplished by lithographic methods, where an auxiliary material (photoresist) is modified requiring additional processes (e.g. etching) to transfer the modification into the material to be structured. Alternatively, the laser light can directly affect the material surface, leading to periodic modification or ablation. In most cases, the generation of a periodic surface relief by ablation is intended, leading to durable high-contrast patterns. The main quality criteria of such patterns are suitable aspect ratio (ratio depth over width of ablated features) and regularity of the structure (absence of defects). To obtain high quality, sufficient control of the interfering beams is necessary. The focus of this paper is on the techniques based on the interference of at least two externally applied beams in contrast to 'laser-induced periodic surface structures (LIPSS),' where one external beam may interfere with internal excitations of the material [5].

A basic method for two-beam interference is the division of the laser beam into two beams by a beam splitter that transmits 50% and reflects 50% of the incoming beam [6–8]. The two beams are recombined on the sample surface, leading to an interference pattern with period $d=\lambda/(2 \sin \alpha)$, with the laser wavelength λ and the angle 2α between the incident beams. The obtained contrast depends strongly on the coherence of the laser source. At sufficiently high fluence and contrast, the interference pattern will lead to an ablated line pattern with period d. Additional splitters generating a third or even more beams lead to two-dimensional interference patterns [9–11]. However, there are a few restrictions concerning the two or multiple beam paths to obtain coherent overlap of the beams on the work piece. First, the beam paths have to be of equal length, and second, in the case of non-perfect spatial coherence, the number of reflections has to be chosen so that the lateral orientations of both beams coincide on the work piece. Moreover, when using short pulses, the length adjustment is rather critical. These restrictions are inherently fulfilled if the recombination of the beams is accomplished by imaging the splitting plane onto the surface. However, in the case of extremely short

***Corresponding author: Jürgen Ihlemann,** Laser-Laboratorium Göttingen e.V., Hans-Adolf-Krebs-Weg 1, 37077 Göttingen, Germany, e-mail: juergen.ihlemann@llg-ev.de. https://orcid.org/0000-0002-7527-882X
Jan-Hendrik Klein-Wiele, Andreas Blumenstein and Peter Simon: Laser-Laboratorium Göttingen e.V., Hans-Adolf-Krebs-Weg 1, 37077 Göttingen, Germany

pulses, the problem remains even with this scheme, that the angle of the pulse fronts of the interfering beams at the sample surface may lead to an insufficient coherence over the full irradiation spot. This problem can be solved if the beam splitter is diffractive instead of reflective. In order to generate two beams, a linear grating can be used as diffractive beam splitter [12, 13]. In principle, this grating can operate in reflection or in transmission. It can be an amplitude or phase grating. For practical and efficiency reasons, transmission phase gratings ('phase masks') are preferably applied [14–16]. In addition to simple linear or crossed gratings, also sophisticated grating systems can be projected onto the work piece by imaging, leading to complex surface patterns [17–19].

Besides imaging of a grating in order to recombine the diffracted beams, also diffractive recombination by a second grating is possible. Such a totally diffractive beam management with a so-called two-grating interferometer has the particular advantage of combining a large patterning field with dramatically reduced requirements concerning beam coherence [20–22].

The simplest approach for interference ablation is a single grating (phase mask) used in contact or proximity mode; i.e. the work piece is placed directly or within a short distance behind this phase mask [23, 24]. If used for material ablation, care has to be taken that the ablated material does not contaminate or damage the phase mask [25].

Another kind of diffractive beam management is given by the application of pixelated diffractive elements [computer-generated holograms (CGHs)]. Because of their flexible design, they are used mostly for the generation of arbitrary, non-periodic patterns. However, for the fabrication of periodic patterns limited to a moderate number of periods, e.g. an array of 10×10 or 20×20 spots, they are rather well suited [26].

Independent of the beam management, the ablation results will strongly depend on the laser pulse characteristics. Obviously, the achievable period depends on the laser wavelength. At the same interference angle, UV beams generate smaller periods compared to visible or infrared (IR) beams. Furthermore, for many materials, the optical absorption is stronger in the UV compared to the longer wavelengths, leading generally to better ablation quality. This is especially the case for widely transparent materials like glasses. However, not only the wavelength but also the pulse duration is of great importance. If the thermal conductivity of the work piece material is high as it is, e.g. in the case of metals, shorter pulses lead to smaller heat-affected zones and, therefore, higher contrast when reducing the structure period. For submicron patterns on metals, only ultrashort (picosecond or femtosecond) pulses are suitable for obtaining satisfying results. A further benefit of using ultrashort pulses is their capability of inducing multiphoton absorption, so that even transparent materials can be treated with visible or IR femtosecond pulses. An example is the fabrication of periodic patterns by two photon polymerization utilizing multibeam interference [27].

In this paper, an overview of results obtained with a femtosecond UV laser system delivering ~500-fs pulses at 248 nm [28] is shown. The combination of short wavelength with short pulse duration facilitates the submicron patterning of metals and semiconductors.

2 Structure formation by interferometric projection

As mentioned above, a system utilizing diffractive optical beam splitting in combination with an imaging optics is very well suited to generate high-resolution deterministic periodic surface structures and is sketched in Figure 1.

The incoming beam is split into multiple beams through a diffractive optical element (DOE), here a beam splitter, which is preferably a high-efficiency phase element. The beam splitter is placed into the object plane of a suitable imaging optics, e.g. a Schwarzschild type objective, and projected onto the sample surface. A beam selector in front of the optics can be used to block or transmit specific beams created by the DOE, enabling the possibility to generate specific patterns if the DOE generates more than two beams. Assuming an aberration-free imaging, the exact temporal and spatial overlap of the selected beams on the sample surface is guaranteed. Thus, a high-quality, homogenous interference pattern can be generated over the whole irradiated area. To obtain a sharp boundary of this area on the sample surface,

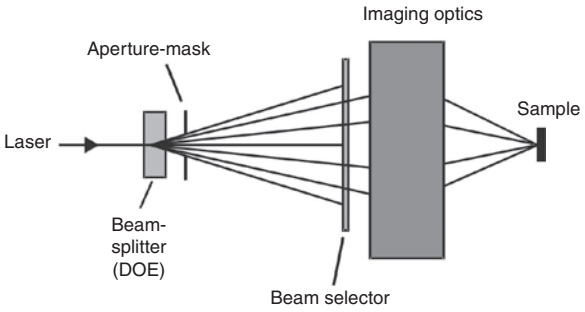

Figure 1: Optical system based on diffractive interferometric projection.

an additional aperture mask is placed very close to the diffraction plane. In order to avoid air breakdown in the focus, the space between the objective and the sample may be flushed with helium. This is necessary especially for large processing fields and high fluences.

3 Calculation of the resulting periodic structures on the sample surface

As mentioned above, the interference pattern generated on the sample surface is purely deterministic, enabling the exact tailoring of desired patterns. To do so, the fluence distribution F is calculated from the superposition of the interfering beams according to

$$F \approx \langle | E_1 + E_2 + E_3 + E_4 \cdots + E_n |^2 \rangle \quad (1)$$

To determine the ablated surface relief S, the material dependent ablation function A of the material must also to be taken into account by taking the composition of F and A, giving

$$S = A \circ F \quad (2)$$

As the ablation behavior of the material has a strong influence on the generated surface structures, the shape and aspect ratio of the ablated structures can be controlled by choosing specific irradiation parameters, namely, the peak fluence per pulse and the number of pulses applied. Figure 2 depicts the situation for a one-dimensional sinusoidal fluence distribution and a simple asymptotic ablation function. Ablation only occurs where the fluence is above the ablation threshold, resulting in a strong deviation from the sinusoidal shape. In this simple case, the width of the resulting flat fillets can precisely be controlled by choosing the correct peak fluence F_{max}.

4 Fabrication of linear gratings

Linear grating patterns are obtained by two beam interference. High-resolution structures with micron or submicron period are preferentially fabricated using a linear phase grating as a DOE- and a Schwarzschild-type objective for imaging [29]. As it is purely reflective without any refractive components, it can be used with high-intensity pulses even in the UV spectral range. If it is used on-axis, the zeroth-order beam is obstructed by the particular mirror arrangement, so that this configuration is specifically suited for ± first-order interference. If the unhindered transmission of the zeroth-order beam is desired, an off-axis arrangement can be used. Gratings on metals and semiconductors [30], optical crystals [31] and optical thin films [32] have been fabricated using such arrangements. Figure 3A displays a relief grating with a 650-nm period ablated in a diamond-like carbon coating by applying 248-nm, 500-fs pulses. In Figure 3A, the surface was irradiated with 10 laser pulses at 200 mJ/cm^2. In Figure 3B, the peak fluence was doubled to 400 mJ/cm^2 and the surface was irradiated with 30 laser pulses, resulting in much narrower fillets and an aspect ratio of more than 2.

5 Fabrication of 'crossed' gratings

Applying a crossed grating mask as the DOE and recombining the four first-order beams (1/0, 0/1, –1/0 and 0/–1) leads to an ablated hole array. A fused silica phase mask specifically designed to maximize the intensity in these diffraction orders while minimizing the zero order was used in this case. Such fused silica phase masks are fabricated with a special process based on laser patterning of silicon sub-oxide (SiO_x) and subsequent oxidation to SiO_2 [33]. Figure 4 shows an array of holes drilled into a 5-µm-thin titanium foil. Dependent on the fluence and number of pulses, through-holes with different diameters ranging

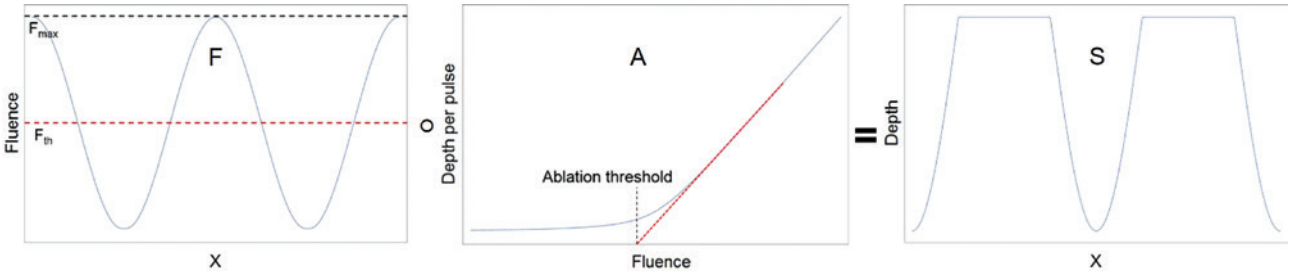

Figure 2: Example for calculating the ablated surface relief S by taking the composition of the interference distribution F and the ablation function A for a maximum fluence $F_{max} = 2F_{th}$.

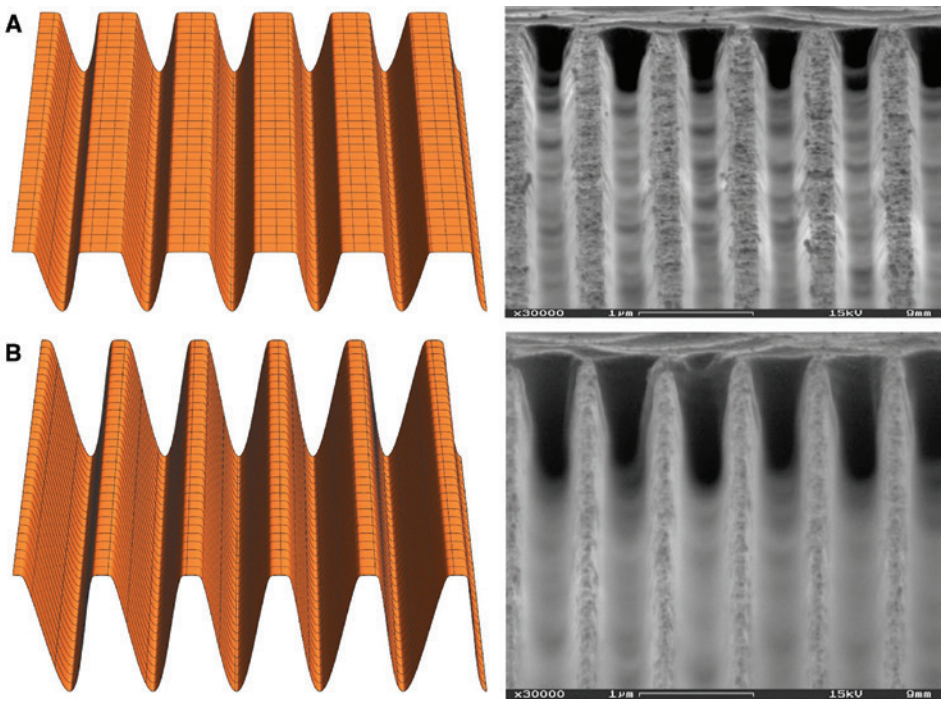

Figure 3: Calculated and experimentally obtained laser ablated gratings on diamond-like carbon coatings with 248-nm, 500-fs pulses for two different irradiation parameters: (A) $F_{max} = 200$ mJ/cm², 10 pulses, (B) $F_{max} = 400$ mJ/cm², 30 pulses.

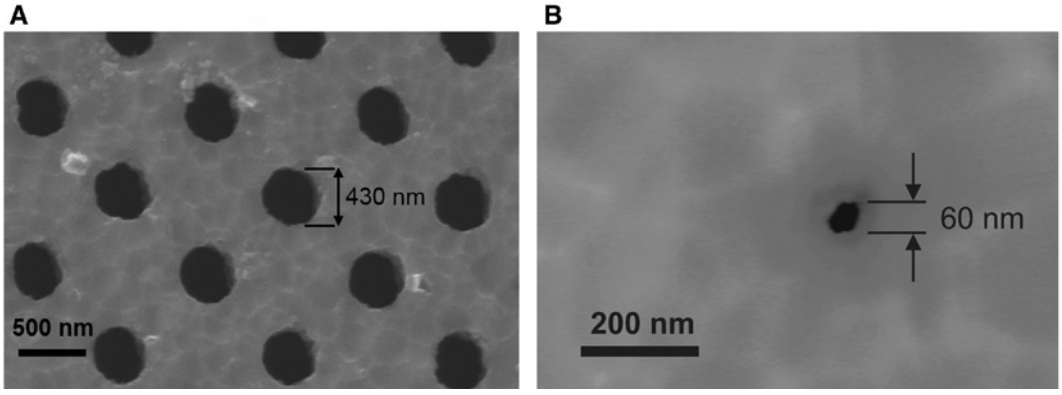

Figure 4: Hole array drilled through a 5-µm titanium foil with 248-nm, 500-fs pulses. (A) $F_{max} = 600$ mJ/cm², 120 pulses, (B) $F_{max} = 150$ mJ/cm², 700 pulses.

from 600 nm down to 60 nm were obtained at the exit side of the foil. To create such small holes, the fluence must be reduced close to the ablation threshold.

6 Circular gratings

Besides line and hole arrays, other types of periodic patterns can also be fabricated. Figure 5 shows a circular ring pattern ablated in hardened steel with 355-nm, 9-ps pulses at peak fluence of 250 mJ/cm². The surface was irradiated with 30 pulses. In this case, an amplitude DOE (chrome on fused silica) consisting of circular rings has been applied, and the first-order diffraction ring was projected onto the surface by a Schwarzschild objective.

7 Phase-controlled multiple beam interferometric projection

An almost unlimited variability of the interference patterns and the resulting surface structures can be obtained by using a diffractive 'pattern generator' comprising multiple independent DOEs and a sophisticated, programmable

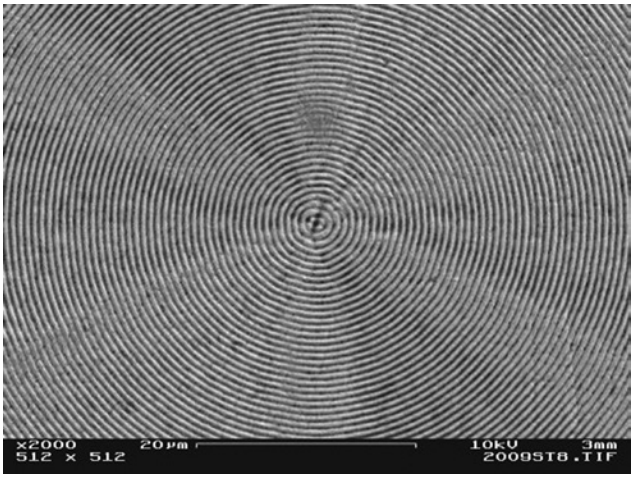

Figure 5: Ring pattern on hardened steel.

beam selector. Because of the distributed diffraction by multiple DOEs, their distance and their rotation angle are further degrees of freedom for the diffractive beam management [19]. Figure 6 shows some examples of patterns generated with this technique.

In a basic configuration, two identical linear gratings are positioned in parallel planes with distance D as sketched in Figure 7.

With the grating lines oriented perpendicular to each other, the path difference between the zero-order and the ± first-order beams diffracted at the first grating under angle α when reaching the second grating amounts to

$$\Delta L = D\left(\frac{1}{\cos\alpha} - 1\right) \tag{3}$$

corresponding to a phase difference of

$$\Delta\phi = \phi_1 - \phi_2 = \frac{2\pi}{\lambda}\Delta L \tag{4}$$

with the wavelength λ. This phase difference between the particular beam pairs generated at the second grating remains constant throughout the further beam propagation and can be finely adjusted by varying the separation D. Similar relations are valid for the other diffracted beams. So, the combination of distance, rotation angle

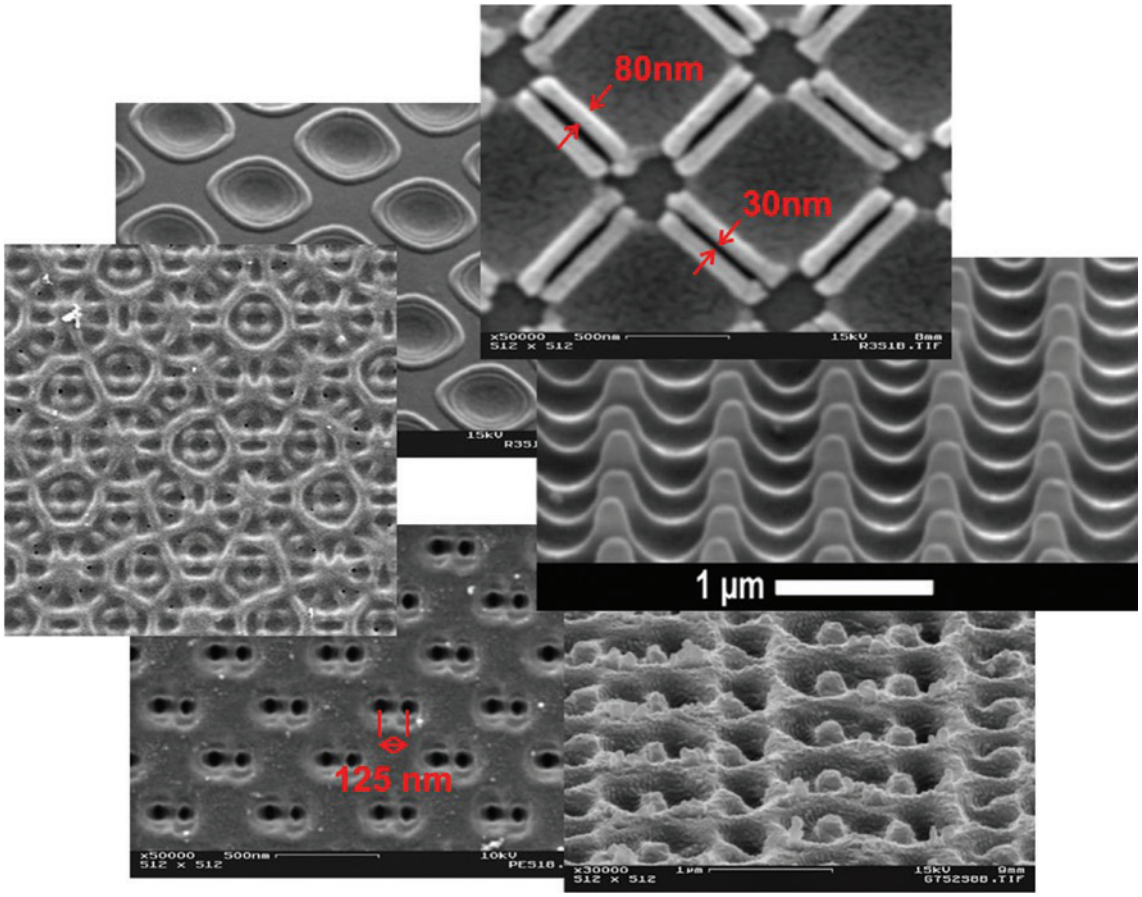

Figure 6: Examples of laser ablated complex periodic patterns obtained by phase-controlled multiple-beam interferometric projection.

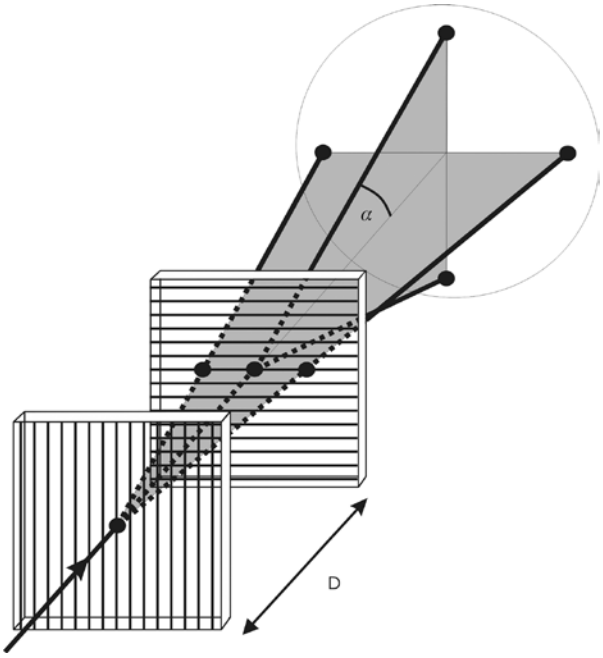

Figure 7: Set of two gratings for the phase-controlled generation of diffracted beams. Distance *D* and rotation of the gratings have influence on the resulting interference pattern.

and selection of specific diffracted beams by blocking the others leads to complex symmetry periodicities, if the beams of such a 'pattern generator' are recombined by imaging onto the work piece. Figure 8 displays patterns fabricated in gallium nitride (GaN) surfaces irradiated with 248-nm, 500-fs pulses, a peak fluence of 250 mJ/cm^2 and three pulses. Three linear phase gratings were used as DOE and the ± first diffraction orders from each of the gratings were selected for interference. The gratings were rotated with respect to each other by an angle of 30°. By changing the subsequent spacing of the gratings, the relative phases of the three beam pairs can be precisely adjusted. Figure 8 shows a case where the distance of gratings 1 and 2 is kept constant. A drastic change of the generated pattern can be obtained by solely varying the longitudinal position of grating 3 and, thus, the phase relation of the corresponding beam pair with respect to the other two. Such patterns can be used, e.g. for material integrated security features for product traceability and counterfeit protection. Similar patterns have been created in order to fabricate photonic quasi-crystals [34].

To demonstrate the excellent predictability of even very complex ablated surface reliefs, Figure 9 shows the comparison between a calculated three-dimensional-surface and a steep-angle (75°) scanning electron microscopy (SEM) image of the corresponding surface structure ablated in GaN. The theoretically predicted surface relief outstandingly matches the measured surface.

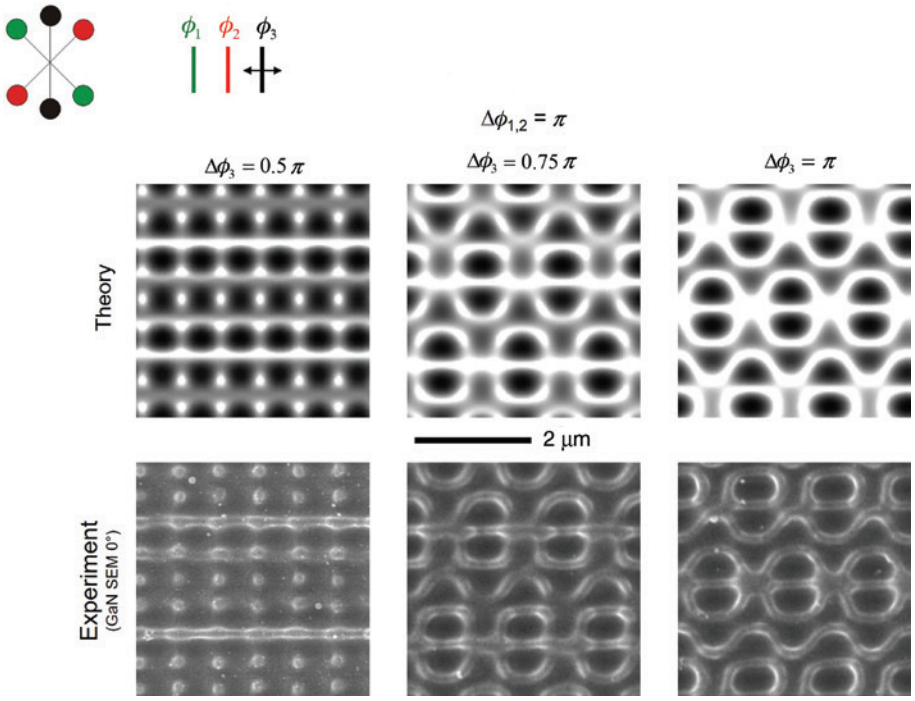

Figure 8: Interference ablation patterns on GaN obtained with six diffracted beams from a set of three crossed gratings. Solely the longitudinal position of the third grating was varied.

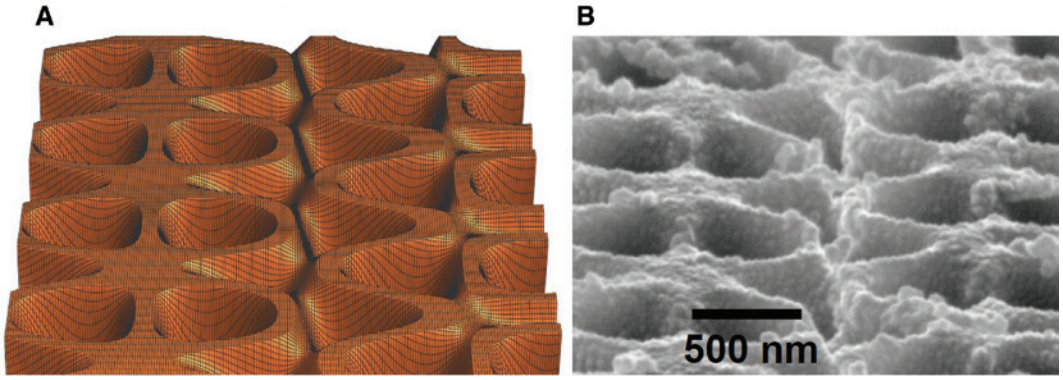

Figure 9: Calculated (left) and ablated (right) complex structures in GaN with $\Delta\phi_{1,2,3}=\pi$, $F_{max}=250$ mJ/cm² and three pulses. The right picture shows an SEM image at an angle of 75°.

8 Two-grating interferometer

Instead of using an imaging optics, the diffracted beams generated at the 'mask grating' can also be recombined by a second grating. In the simplest case, the ± first-order beams generated at a linear transmission grating G1 with period p are again diffracted at a second grating G2 with period $p/2$ (Figure 10). If the lines of both gratings are oriented parallel to each other, and the distance between G1 and G2 is d, at the same distance d behind G2, an interference pattern with period p is obtained [35]. A corresponding line structure can be ablated if the work piece is placed in this plane. Because of this specific arrangement, the characteristics of the diffraction pattern do not depend on the wavelength or the coherence properties of the used laser. In front of such a two-grating interferometer, an arbitrary optical system can be used to shape the beam. Most simply, in order to achieve high fluence on the work piece sufficient for material ablation, a (cylindrical) condenser lens can be used. However, if the zero-order beam behind G1 carries some residual energy, this beam shaping has to be arranged so that this zero-order beam can be blocked to achieve undisturbed two-beam interference. Similar two-grating interferometers have been used for lithographic illumination [36] and for fiber Bragg grating recording [37].

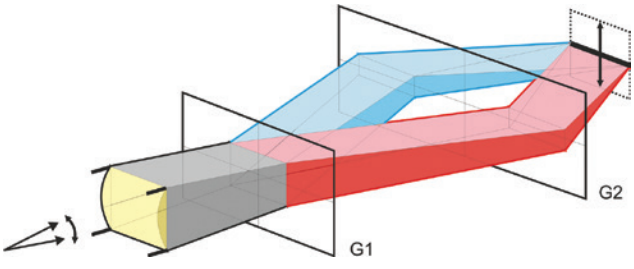

Figure 10: Two-grating interferometer with periods $p_1(G1)=2p_2(G2)$ with cylindrical focusing to obtain a line focus modulated horizontally with p_1.

This method is especially suitable for large-area patterning. The size of the area that can be structured without stitching artefacts is only limited by the sizes of the gratings. Figure 11 displays a line pattern on a steel surface fabricated with this method. The area shown in Figure 11A can be processed within a few seconds. Direct writing of such a grating instead of interference processing would take much longer. Whereas direct writing with a laser spot of a few-micron diameter over such a field can be extremely fast due to fast scanners and suitable objectives, direct writing with a submicron spot is much more challenging. To obtain submicron spot sizes, high numerical aperture microscope objectives are required, which are only available with field diameters of typically less than 1 mm. These small processing fields have then to be stitched together with very high precision, slowing down the overall process speed significantly.

9 Diffractive optical element (CGH)

CGHs are pixelated DOEs designed by computer calculations to reproduce a predetermined intensity distribution when irradiated with a specified light source. Such design calculations are performed, e.g. on the basis of iterative Fourier transform algorithms (IFTA) [38, 39]. For high-power laser applications, usually transmission phase elements in the form of transparent substrates bearing a specific height profile are applied. CGHs are often used to create non-periodic, image-wise patterns, but also for creating periodic patterns, e.g. in the form of multi-spot arrays they can be used. The advantage compared to simple grating-like elements is that the

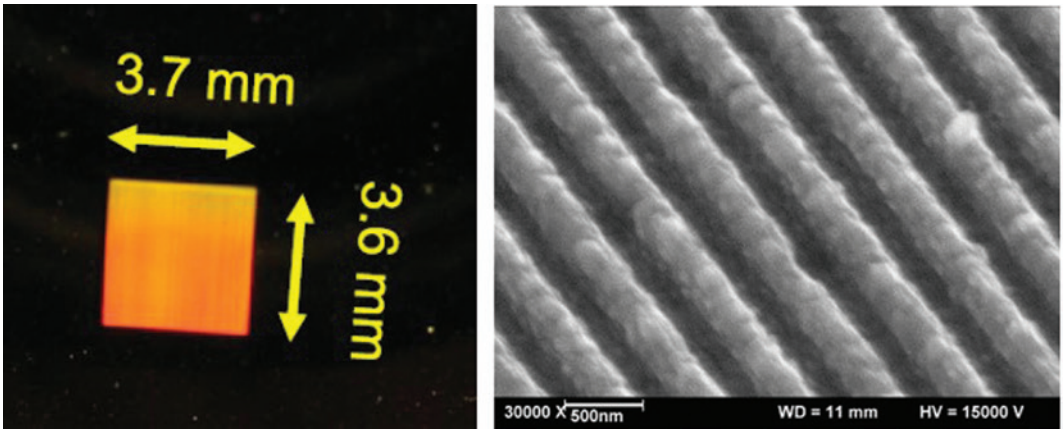

Figure 11: Linear gratings fabricated with a two-beam interferometer: steel, period 475 nm, 80 mJ/cm², size 3.7×3.6 mm², 1660 pulses.

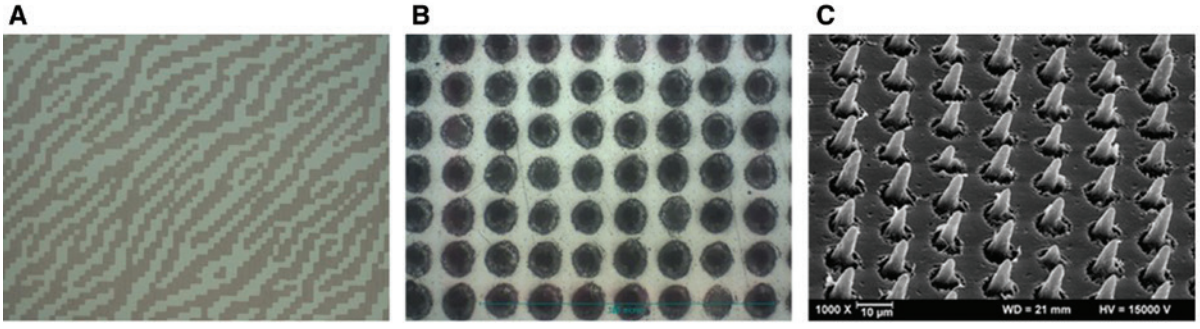

Figure 12: Fabrication of periodic surface patterns with CGH. (A) Detail of the CGH pattern; (B) hole array in steel mold fabricated with 50 pulses at 1 J/cm²; (C) replicated polypropylene spike array.

period of the pattern and the size of a single spot are decoupled. This means that an array of small spots with comparatively large distance between the spots can be achieved.

As an example, the application of a CGH for fabricating a superhydrophobic surface is presented [2]. Figure 12A displays a section of a CGH calculated by IFTA and fabricated by the above-mentioned laser process. The CGH is designed to create a 25×25 spot array from one incoming UV-fs laser beam. This spot array is imaged onto the steel work piece in order to drill 25×25 holes in parallel (Figure 12B). Fast patterning of large areas is possible by assembling many arrays with 625 holes each side by side. From this patterned steel part, plastic spike arrays (Figure 12C) with super hydrophobic behavior are molded (Figure 13).

10 Proximity processing

For patterning applications, where only moderate fluences are required, another simple method can be applied. The work piece to be patterned is placed directly behind the phase grating, which is irradiated with the laser beam, so that the sample surface is at a position where the propagating diffracted beams are not yet separated (Figure 14).

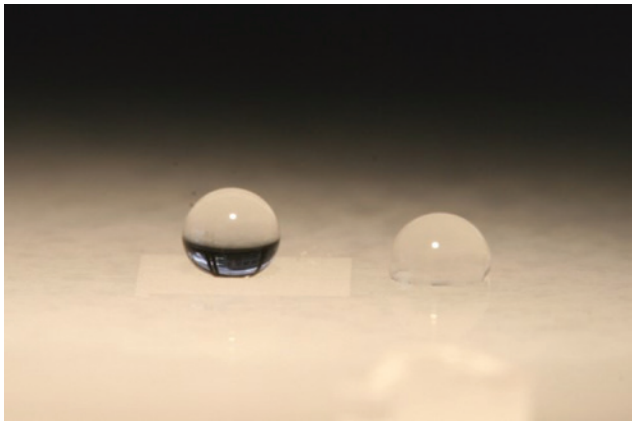

Figure 13: Change in wettability of polypropylene surface: the original surface (right) turns to superhydrophobic (left) on the molded area with a spike array structure.

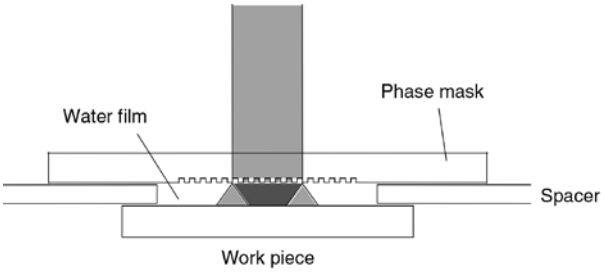

Figure 14: Arrangement for proximity processing: the 130-µm space between the phase mask and work piece is flushed with water.

The conditions for obtaining high-contrast interference ablation with this method are as follows:

1. The fluence that can be transmitted by the phase mask without damage is sufficient for ablation. (There is no fluence increase like elsewhere by demagnification or focusing.)
2. The spatial coherence of the laser beam is sufficient to generate good contrast even in a suitable distance behind the phase mask [23].
3. Measures are taken to avoid contamination or damage of the phase mask by the ablated product plume.

Figure 15 shows an example of this processing method. A silicon surface is structured with a line pattern having a period of 1 µm. The space between the phase mask and the work piece (distance: 130 µm) is flushed with water to prevent debris deposition on the phase mask and on the work piece. The phase mask profile has to be specifically adjusted for use in water, as the refractive index is different from that in air. Furthermore, a pulse length of 1.3 ps is chosen here, as too short pulses would lead to nonlinear effects in the fused silica material of the phase mask. The dominant structure period depends on the contribution of the residual zero-order beam and the ablation threshold behavior [25, 40].

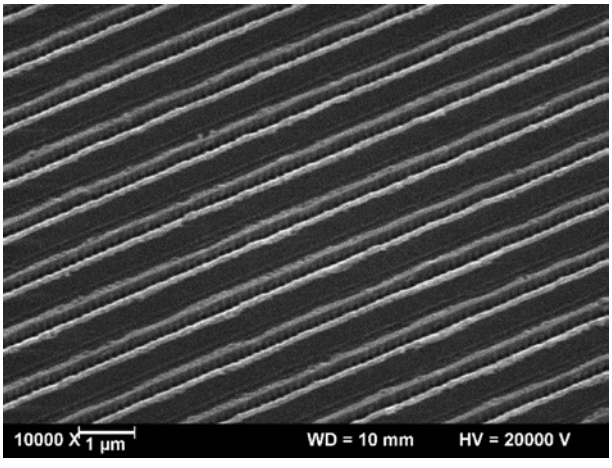

Figure 15: Line pattern on silicon obtained by proximity processing, 120 mJ/cm², 20 pulses (248 nm, 1.3 ps).

11 Structure formation process

Understanding the mechanisms leading to laser-induced structure formation on the micron and submicron scale can help to optimize the adaptation of surface structures to specific functionalities. A hybrid atomistic-continuum model capable of capturing the essential mechanisms responsible for the nanostructuring process is used to model the interaction of a single spatially modulated laser pulse with a metal (gold) target [41]. It allows an insight in the evolution of structural details on the surface and beneath over a time scale of a few picoseconds to nanoseconds after irradiation, which are mostly hidden to experimental investigation methods. The model consists of two parts: the atomic motion is described within a molecular dynamics (MD) approach, whereas a diffusion differential equation for electrons accounts for the effect of free carriers with regard to their temperature dynamics. This approach allows a direct comparison of theory-based model calculations with experimental results. In the experiment, a two-beam interference pattern with a period of 500 nm is generated using an ultrashort pulse excimer laser at a wavelength of 248 nm (Figure 16). To reduce the computed volume to a minimum, a thin slice geometry comprising one period of the sinusoidal intensity pattern is used, so that a comparison of the computational and experimental results on the same length scale is possible.

At two fluence levels of 125 and 150 mJ/cm² around the melting threshold, a comparison of the simulation and the experiment at a pulse length of 1.6 ps is given in Figure 17. Figure 17A and B display the SEM top view perspectives, and Figure 17C and D show the transmission electron microscopy (TEM) cross-sectional views. The formation of subsurface voids can be observed both in the simulation and the experiment. The simulation allows the understanding of the formation process of the voids by looking at different time steps at 100 and 500 ps after irradiation. Starting with the formation of small voids in an overheated melt, followed by their coalescence in (e) and (f), the process ends with recrystallization of the melt with a single (g) or separated voids (h). There is remarkable agreement of experimental and simulation results.

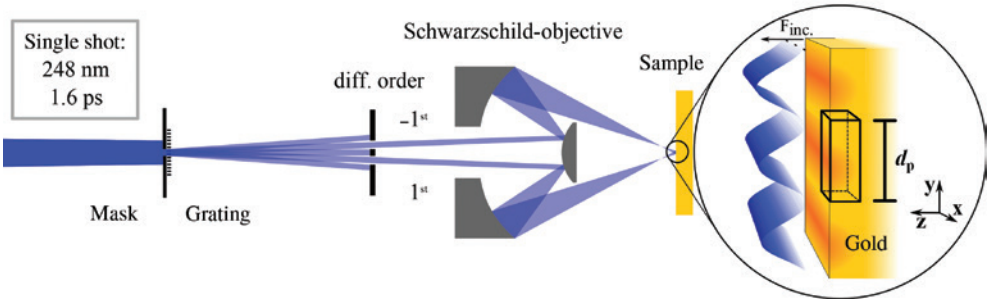

Figure 16: Mask projection setup leading to a sharp sinusoidal intensity profile on the sample and depicted modeling volume (black box).

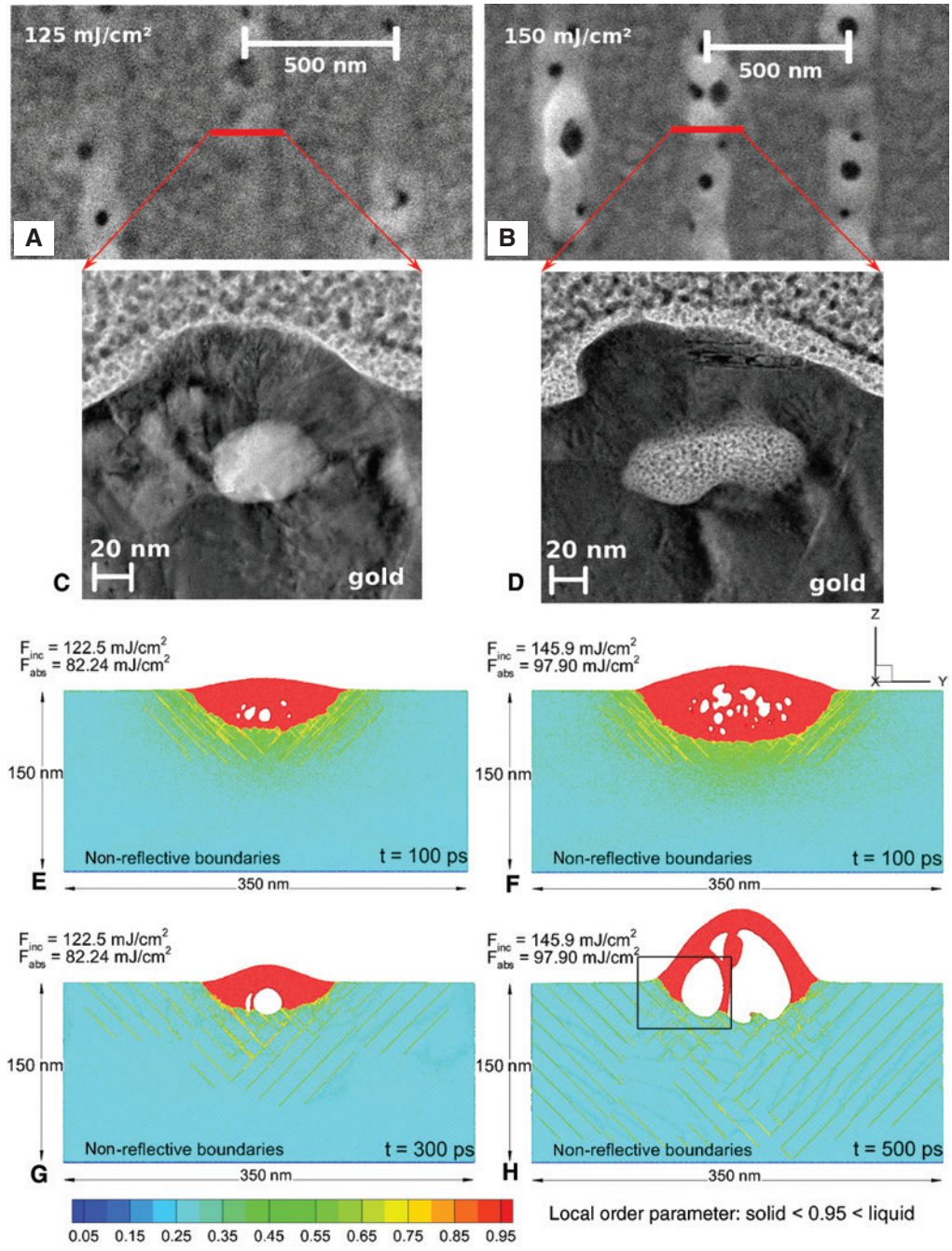

Figure 17: Structure formation in experiment and theory: SEM (A, B), TEM cross sections (C, D) and simulated cross sections (E–H) for two laser fluences: 125 mJ/cm² (left column) and 150 mJ/cm² (right column). Figure taken from reference [41].

12 Conclusion

In conclusion, various interference-based techniques for the fabrication of micro- an nano-patterns are presented. Applying diffractive beam management, high-definition, strictly periodic structures are obtained with a vast variety of different topologies. The applied UV pulses of pico- and subpicosecond duration ensure well-defined patterning of various materials including metals, semiconductors and dielectrics with structural details well below the micron level. A simple phenomenological model gives a good prediction of the shape of complex patterns, which are obtained experimentally. A much more sophisticated atomistic model can even describe the structural details on the submicron level on and below the processed surface. Detailed knowledge of the structure formation and the capability to predict overall topologies provide a powerful tool for designing the surface structures for specific functionalities.

Acknowledgment: The present work was supported by the Deutsche Forschungsgemeinschaft (DFG; grants IH 17/18-1 and IH 17/18-2, Funder Id: http://dx.doi.org/10.13039/501100001659).

References

[1] J.-H. Klein-Wiele and P. Simon, Mikroproduktion 04/18, 60 (2018).
[2] J. Bekesi, J. Kaakkunen, W. Michaeli, F. Klaiber, M. Schoengart, et al., Appl. Phys. A 99, 691 (2010).
[3] S. Rung, K. Bokan, F. Kleinwort, S. Schwarz, P. Simon, et al., Lubricants 7, 43 (2019).
[4] L. Müller-Meskamp, Y. H. Kim, T. Roch, S. Hofmann, R. Scholz, et al., Adv. Mater. 24, 906 (2012).
[5] J. Bonse, S. Höhm, S. V. Kirner, A. Rosenfeld and J. Krüger, IEEE J. Sel. Top. Quant. Electron. 23, 9000615 (2017).
[6] K.J. Ilcisin and R. Fedosejevs, Appl. Opt. 26, 396 (1987).
[7] T. Lippert, T. Gerber, A. Wokaun, D. J. Funk, H. Fukumura, et al., Appl. Phys. Lett. 75, 1018 (1999).
[8] S. Pissadakis, L. Reekie, M. N. Zervas and J. S. Wilkinson, J. Appl. Phys. 95, 1634 (2004).
[9] C. Daniel, F. Mücklich and Z. Liu, Appl. Surf. Sci. 208, 317 (2003).
[10] S. Beckemper, J. Huang, A. Gillner and K. Wang, J. Laser Micro. Nanoeng. 6, 49 (2011).
[11] J. Huang, S. Beckemper, A. Gillner and K. Wang, J. Micromech. Microeng. 20, 095004 (2010).
[12] P. E. Dyer, R. J. Farley and R. Giedl, Opt. Commun. 115, 327 (1995).
[13] H. M. Phillips and R. A. Sauerbrey, Opt. Eng. 32, 2424 (1993).
[14] P. E. Dyer, R. J. Farley, R. Giedl and D. M. Karnakis, Appl. Surf. Sci. 96–98, 537 (1996).
[15] M. Mäder, T. Höche, J. W. Gerlach, R. Böhme and B. Rauschenbach, Phys. Stat. Sol. B 247, 1372 (2010).
[16] R. J. Peláez, C. N. Afonso, J. Bulíř, M. Novotný, J. Lančok, et al., Nanotechnology 24, 095301 (2013).
[17] J.-H. Klein-Wiele and P. Simon, Appl. Phys. Lett. 83, 4707 (2003).
[18] S. Indrišiūnas, B. Voisiat, M. Gedvilas and G. Račiukaitis, J. Micromech. Microeng. 23, 095034 (2013).
[19] J.-H. Klein-Wiele, T. Fricke-Begemann, P. Simon and J. Ihlemann, Opt. Expr. 27, 28902 (2019).
[20] J. Bekesi, P. Simon and J. Ihlemann, Appl. Phys. A 114, 69 (2014).
[21] J. J. J. Kaakkunen, K. Paivasaari and P. Vahimaa, Appl. Phys. A 103, 267 (2011).
[22] Y. Bourgin, S. Bakkali, Y. Jourlin, S. Tonchev and O. Parriaux, Opt. Lett. 34, 3800 (2009).
[23] P. E. Dyer, R. J. Farley, R. Giedl, C. Ragdale and D. Reid, Appl. Phys. Lett. 64, 3389 (1994).
[24] K. Tsunetomo and T. Koyama, Opt. Lett. 22, 411 (1997).
[25] B. Borchers, J. Békési, P. Simon and J. Ihlemann, J. Appl. Phys. 107, 063106 (2010).
[26] J. Kaakkunen, J. Bekesi, J. Ihlemann and P. Simon, Appl. Phys. A 101, 225 (2010).
[27] T. Kondo, S. Matsuo, S. Juodkazis, V. Mizeikis and H. Misawa, Appl. Phys. Lett. 82, 2758 (2003).
[28] J. Bekesi, S. Szatmári, P. Simon and G. Marowsky, Appl. Phys. B 75, 521 (2002).
[29] P. Simon and J. Ihlemann, Appl. Phys. A 63, 505 (1996).
[30] P. Simon and J. Ihlemann, Appl. Surf. Sci. 109/110, 25 (1997).
[31] K. Chen, J. Ihlemann, P. Simon, I. Baumann and W. Sohler, Appl. Phys. A 65, 517 (1997).
[32] F. Beinhorn, J. Ihlemann, P. Simon, G. Marowsky, B. Maisenhölder, et al., Appl. Surf. Sci. 138–139, 107 (1999).
[33] J. Ihlemann, J.-H. Klein-Wiele, J. Békési and P. Simon, J. Phys. Conf. Ser. 59, 449 (2007).
[34] G. Zito, B. Piccirillo, E. Santamato, A. Marino, V. Tkachenko, et al., Opt. Expr. 16, 5164 (2008).
[35] J. Békési, J. Meinertz, J. Ihlemann and P. Simon, Appl. Phys. A 93, 27 (2008).
[36] A. Yen, E. H. Anderson, R. A. Ghanbari, M. L. Schattenburg and H. I. Smith, Appl. Opt. 31, 4540 (1992).
[37] M. Livitziis and S. Pissadakis, Opt. Lett. 33, 1449 (2008).
[38] J. Turunen and F. Wyrowski, Diffractive optics for industrial and commercial applications (Akademie Verlag, Berlin, 1997).
[39] J. Bekesi, D. Schäfer, J. Ihlemann and P. Simon, Proc. SPIE 4977, 235 (2003).
[40] Z. Xiong, G. D. Peng, B. Wu and P. L. Chu, J. Lightwave Technol. 17, 2361 (1999).
[41] D. S. Ivanov, V. P. Lipp, A. Blumenstein, F. Kleinwort, V. P. Veiko, et al., Phys. Rev. Appl. 4, 064006 (2015).

Jan-Hendrik Klein-Wiele
Laser-Laboratorium Göttingen e.V.
Hans-Adolf-Krebs-Weg 1, 37077 Göttingen
Germany
juergen.ihlemann@llg-ev.de. https://orcid.org/0000-0002-7527-882X

Jan-Hendrik Klein-Wiele received his diploma in physics (1997) from the University of Göttingen. During his diploma, he was working at the Max-Planck-Institute for fluid dynamics in the group of Prof.

Tönnies, examining ultrafast optical excitations on sodium cluster films. In 1997, he joined Laser-Laboratorium Göttingen, Germany, where he dedicated his research to the fabrication of periodic nanostructures by direct ultrashort pulse laser ablation. His work includes time-resolved studies of the ablation process, the development of sophisticated optical systems for periodic nanostructuring and the industrial and scientific applications of such structures.

Andreas Blumenstein
Laser-Laboratorium Göttingen e.V.
Hans-Adolf-Krebs-Weg 1, 37077 Göttingen
Germany

Andreas Blumenstein received his B.Sc. in (2011) and M.Sc. in (2013) both in physics from the University of Göttingen. He received his Ph.D. from the University of Kassel in (2019). For his thesis, he worked at the Laser-Laboratorium Göttingen, Germany, investigating ultrashort laser pulse surface nanostructuring and the role of non-equilibrium effects on the energy absorption process. Further research interests are the creation and application of few cycle laser pulses using stretched flexible hollow core fibers.

Peter Simon
Laser-Laboratorium Göttingen e.V.
Hans-Adolf-Krebs-Weg 1, 37077 Göttingen
Germany

Peter Simon received his diploma and Ph.D. degrees in Physics from the University of Szeged in 1982 and 1986, respectively. In 1988, he joined the Laser-Laboratorium Göttingen, where he participated in research associated with the generation, amplification and characterization of femtosecond laser pulses and their application for materials processing. In 1992, he was appointed as a group leader of the High Intensity Laser Technology Group and in 2005 as the Head of the Department of Ultrashort Pulse Photonics. Since 2015 he is heading the Department Short Pulses/Nanostructures. The subjects of his current research include the generation and amplification of ultrashort laser pulses, the compression of energetic few-cycle pulses and the submicron-scale surface texturing of technical materials.

Jürgen Ihlemann
Laser-Laboratorium Göttingen e.V.
Hans-Adolf-Krebs-Weg 1, 37077 Göttingen
Germany

Jürgen Ihlemann received his diploma in physics (1984) and Ph.D. in physical chemistry (1987) from the University of Göttingen. From 1984 to 1988, he was with the the Max-Planck-Institute for biophysical chemistry, Göttingen, where he was working on picosecond laser spectroscopy. In 1989, he joined Laser-Laboratorium Göttingen, Germany, where he is now head of the nanostructure technology group. Research interests are UV laser micro- and nanomachining, patterning of surfaces and thin films and ultrashort pulse laser ablation.